Korean J. Chem. Eng., 35(2), 613-620 (2018)
DOI: 10.1007/s11814-017-0291-y

pISSN: 0256-1115
eISSN: 1975-7220

Some general aspects of a gas-solid fluidized bed using digital image analysis

Mahdi Salehi-Asl, Saeed Azhgan, and Salman Movahedirad†

School of Chemical Engineering, Iran University of Science and Technology, P. O. Box 16765-163, Tehran, Iran
(*Received 8 April 2017 • accepted 15 October 2017*)

Abstract−Digital image analysis (DIA) was used to achieve some information related to aspect ratio of the bubbles, bed expansion fluctuations and the emulsion area at different gas velocities and different bed heights. All experiments were done in a pseudo-2D gas-solid fluidized bed. Variations of the bubble fraction at different gas velocities and different bed heights were investigated. It was found that when the excess gas velocity increases, the dimensionless bed height increases linearly with slope of about 0.4 for LLDPE particles. To validate the analysis, the bubble diameter achieved by DIA results in this work was compared with the bubble diameter correlation presented by Shen et al. Bubble aspect ratio in different heights of the bed was extracted through image analysis, and it was observed that the bubble aspect ratio first increases with the bed height and near the freeboard becomes flattened. Results of the experiments show that the emulsion phase becomes more expanded at higher excess gas velocities. As demonstrated by the analysis results, by increasing the bed height, bubble fraction parameter is decreased.

Keywords: Fluidized Bed, Digital Image Analysis, Bubble, Emulsion Phase

INTRODUCTION

Fluidization is a unit operation by which solid particles behave as a fluid through a suspension in a gas or liquid phase. Fluidization is preferable in many chemical industries because of its excellent mixing characteristics and increased contact area between desired phases, resulting in better heat and mass transfer [1].

Most of the characteristics of fluidized beds, such as their excellent heat and mass transfer properties, are related to the presence of bubbles inside the bed. Therefore, the study of gas bubble behavior is important for the purpose of fluidized bed reactor design [2].

In the past few decades, there has been great progress in the capacity of computer processors, making it possible to simulate complicated systems. But it is obvious that in order to validate the models used in the computer simulations, more accurate and detailed quantitative experimental data are necessary [3]. Different techniques for probing the dynamics of fluidized bed have been developed to achieve reliable experimental data sets. The probing methods are classified into two groups depending on the nature of the probes contacting the bed: intrusive or none-intrusive. The application of intrusive techniques causes great errors by the probe interfering, but none-intrusive techniques provide good results with less error. The intrusive techniques are largely based on electrical resistance, impedance, inductance, piezoelectric or thermal probes, while the non-intrusive techniques are mostly based on photographic, X-ray, light scattering or laser techniques [4].

Advanced digital imaging systems have led to an increase in the application of digital imaging in the study of lab-scale fluidized beds. Digital image analysis (DIA) is particularly suitable for pseudo-2D gas-solid fluidized beds where the inter-phase boundary is easy to detect and the effect of bed depth is minimal [3].

Mori et al. [5] developed a correlation of the bubble size growth in fluidized beds. They determined a maximum bubble diameter. Rowe et al. [6] presented some results about bubbles in cylindrical beds using the X-ray photography. They presented measurements of shapes, sizes, and velocities of bubbles in beds of different particles such as spherical glass ballotini, irregular natural sand and several other materials. They observed that both the size of the bubble wake and its velocity depend on the size and the shape of the fluidized particles.

Kuipers et al. [7] employed earlier developed hydrodynamic model of gas-fluidized beds to investigate bubble formation at a single orifice in a two-dimensional bed. They compared theoretically predicted measurements for bubble sizes, formation times and shapes with experimental data obtained from triggered photographs. They concluded from both the experimental and theoretical results that a strong leakage of bubble gas into the emulsion phase occurs, especially during the initial stage of bubble formation. Additionally, they investigated the effect of solid particle properties on the bubble formation.

Lim et al. [8] developed a method based on digital image analysis to measure the bubble properties in gas-solid fluidized beds. They have presented results related to distribution of various bubble properties, including bubble size, shape factor and aspect ratio, as a function of bed height and fluidization velocity. Hull et al. [9] developed semi-empirical correlations for the average size and rise velocity of bubbles in a 2D-bubbling fluidized bed with and without simulated horizontal tube bundles, using digital images captured with a CCD camera. Caicedo et al. [10] used data collected from a CCD camera to find the effect of reduced velocity on the shape factor and aspect ratio of bubbles formed in a pseudo-2D fluidized bed. Goldschmidt et al. [11] developed a whole-field, non-

†To whom correspondence should be addressed.
E-mail: movahedirad@iust.ac.ir, movahedirad@gmail.com

intrusive digital image analysis technique to enable measurement of bed expansion and segregation dynamics of colored particles in dense pseudo-2D gas-solid fluidized bed. They showed that even small bubbles and voidage waves could be detected with their method. Shen et al. [12] used image processing toolbox of MATLAB to achieve a high level of automation in the acquisition, process and analysis of digitized images of pseudo-2D bubbling fluidized beds captured with a digital video camera. Laverman et al. [13] investigated the hydrodynamics of a freely bubbling pseudo-2D fluidized bed experimentally for different bed aspect ratios at different superficial gas velocities using a combination of particle image velocimetry (PIV) and DIA. Coupling of both DIA and PIV measuring techniques led to the information on both the bubble behavior and emulsion phase circulation patterns simultaneously. Busciglio et al. [14] compared DIA method and numerical simulation of fluidized bed. They showed that bubble aspect ratio is near 1 for most of the bubbles in different gas velocities. Also, an increase in the skewness of the aspect ratio distribution was observed with increasing inlet gas velocity. Asegehegn et al. [15] investigated bubble behavior in fluidized beds with and without immersed horizontal tubes using DIA technique. They reported that in the bed without immersed tubes the bubble aspect ratio increases with increasing of the particle size. Movahedirad et al. [16] studied the bubble size distribution in a pseudo-2D fluidized bed. Other phenomena such as bubble splitting and coalescence have been investigated using DIA [17]. Olaofe et al. [3] adopted enhanced capacities of state-of-the-art photographic instruments in a new DIA method to evaluate local particle composition and segregation degree in a lab-scale pseudo-2D gas-solid fluidized bed. Furthermore, newly developed DIA technique presented by them permits the simultaneous evaluation of the bubble size and position. Guardiola et al. [18] presented an experimental study to measure the bed height of a 2D gas-solid fluidized bed using computer vision. Minimum fluidization velocity and bed expansion were measured with high precision in their work as well.

In the present work some general aspects of a pseudo-2D gas-solid fluidized bed have been studied using DIA. Size and aspect ratio of bubbles, bed expansion and its surface fluctuations, the bubble fraction and the emulsion phase area at different gas velocities in a pseudo-2D gas-solid fluidized bed have been studied.

EXPERIMENTAL

Linear low-density polyethylene (LLDPE) particles (d_p=1.0-1.3 mm) was used as the bed material with the approximate sphericity of one. The particles were filled in a 0.30-m wide pseudo-2D fluidized bed with 0.8-m height and the bed thickness was 0.015 m. The initial height of particles in the bed was 0.30 m. The particles were in the B category based on Geldart's classification [19]. A schematic representation of the experimental setup is given in Fig. 1.

Compressed air premixed with steam (75-90% relative humidity) was fed to the bed as a fluidizing gas stream. The inlet flow was injected into the bed through a porous plate distributor attached to the bottom of the pseudo-2D bed.

To achieve clear images, a black curtain was placed in the back side of the bed and the front side was illuminated by halogen bulbs as shown in Fig. 1.

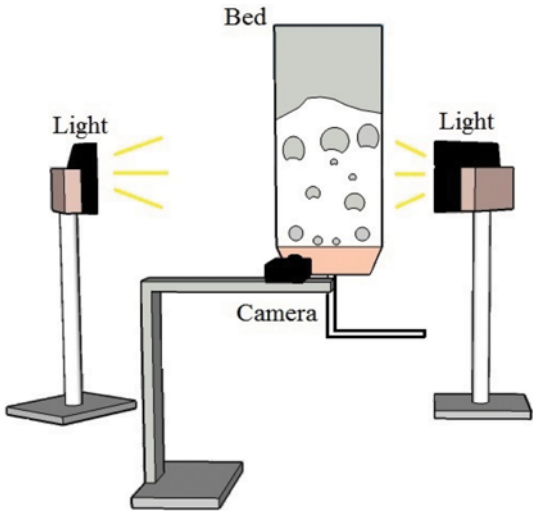

Fig. 1. Schematic representation of the experimental setup.

Table 1. Experimental conditions and camera settings

Experimental minimum fluidization velocity u_{mf} [m/s]	0.24
Bed dimension W×D×H [m×m×m]	0.3×0.015×0.7
Particle size [mm]	1.0-1.3
Delay time between images [s]	0.0059
Relative humidity of inlet air [%]	75-90
Particle density ρ_p [kg/m^3]	920

To take images from the pseudo-2D fluidized bed, a LaVision ImagerPro high-speed CCD camera was used. The shutter speed of the camera was adjusted by an oscillator connected to the computer. Main experimental conditions and camera settings are summarized in Table 1.

It is necessary to consider an important point about the particles and the wall effect in fluidized beds; front/back wall effects exist for all sizes of particles. But to have a reliable experimental data set, the prevention of "*bridge formation*" is necessary in a pseudo-2D fluidized bed. Link et al. [20] have shown that a minimum thickness of about six-times of particle diameter is adequate for prevention of the bridge formation in a pseudo-2D fluidized bed. In the present study, assuming d_p=1.1 mm, the bed thickness is about 13-14 times of particle diameter, which is sufficient for prevention of bridge formation according to the DPM study of Link et al. [20].

DIGITAL IMAGE ANALYSIS

1. Procedure

The DIA technique was applied to detect bubble properties in terms of position, size and shape; also the same technique was used to determine the emulsion phase properties such as area of emulsion and the bed expansion. After recording the video of bubbles rising through the pseudo-2D fluidized bed, the captured video was converted into many images forming frame by frame of the pro-

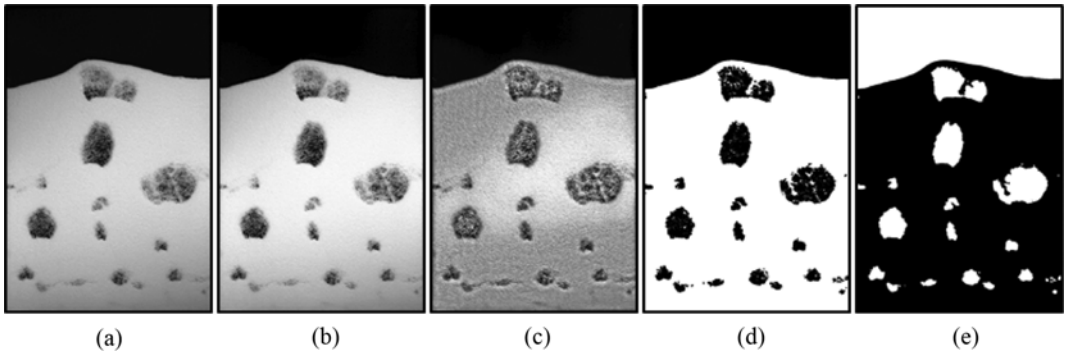

Fig. 2. Digital image analysis steps: (a) original image (b) after normalization (c) after local contrast enhancement (d) after threshold step (e) final binary image.

cess. Then, bubble phase could be separated from the emulsion phase by image processing techniques.

In this work the software applied for image processing method was ImageJ [21], a free software with high features that make it possible to process too many images with reliable results. The convenience of working with software was the main purpose of our choice. The software lets us to apply various image processing steps on a specific image and do the same procedure for the other images. According to our image processing procedure, the first main step after cropping the images was to normalize images that let us have images with more uniform intensity, as done by Laverman et al. [13]. The second main step was to enhance local contrast, which was very helpful to distinguish bubble phase from emulsion phase. The next step was to make binary the processed images, i.e., based on a threshold value. The threshold value is obtained from IsoData method, which is an iterative selection method for image threshold detection [21,22]. Fig. 2 shows the image processing procedure details, applied on a sample image.

2. Bed Height

Bed height and its fluctuation are two important parameters of fluidized beds which can be used in fluidized bed design considerations. Bed height in this work was obtained by fitting a curve to the freeboard and then averaging from the height of the pixels over this curve. The bed height then calculated using Eq. (1):

$$h = \frac{\Sigma_{i=0}^{N_{pix}} y_{pix,\,i}}{N_{pix}} \tag{1}$$

where h is the bed height, N_{pix} is the number of pixels which form the freeboard curve and y is the vertical position of each pixel.

Fig. 3 shows the freeboard fitted curves for two consecutive images when a bubble exits from the bed. As can be observed from this figure, the bed height is significantly reduced when the bubble leaves the bed.

3. Bubble Aspect Ratio

One of the bubble properties is its shape, which is defined as the bubble aspect ratio. Bubble aspect ratio is defined as the vertical to horizontal length ratio of a bubble, as shown in Fig. 4.

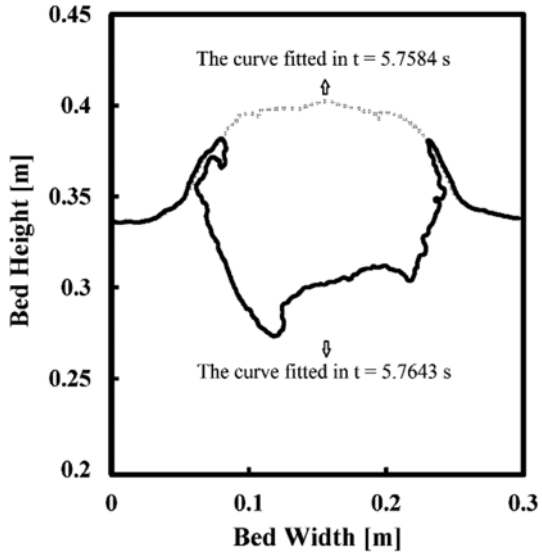

Fig. 3. Evaluation of bed height using curve fitted on top of the bed.

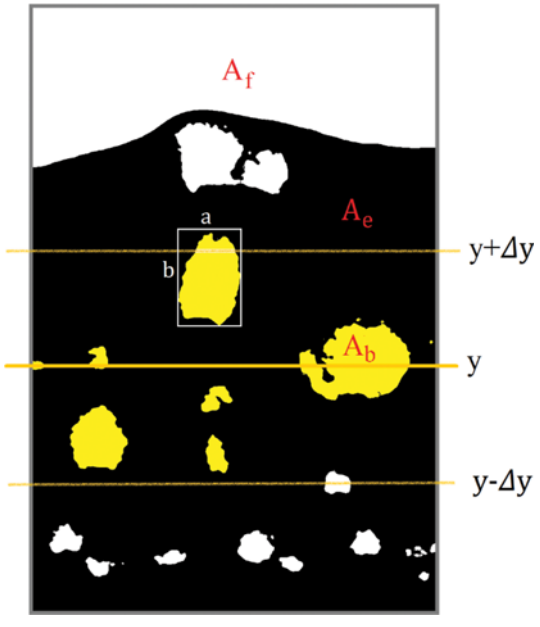

Fig. 4. Dimension of bubbles in order to calculate aspect ratio, along with the definition of control volume for averaging operation and different areas in bed.

$$\text{Aspect ratio} = \frac{b}{a} \tag{2}$$

To study the change of bubble aspect ratio through the bed at different heights, some control volumes are considered through the bed height as shown in Fig. 4, and the averaged value of the bubbles aspect ratio is reported for each control volume. The same method was used for other parameters such as bubble diameter and fraction of the bubbles in the bed.

4. Bubble Fraction in the Bed

In this work δ is defined as the fraction of bubble area to the whole bed area. Bubble area, emulsion phase area and whole bed area are shown in Fig. 4. A_f, A_e and A_b are freeboard, emulsion phase and a single bubble areas, respectively. These parameters can be calculated by image processing as described earlier. Bubble fraction in the bed is calculated by Eq. (3).

$$\delta = \frac{\Sigma_{i=1}^{N_b} A_{b,i}}{A_e + \Sigma_{i=1}^{N_b} A_{b,i}} \tag{3}$$

RESULTS AND DISCUSSION

Four gas flow rates, including 1.25-, 1.5-, 1.75- and 2.0-times the minimum fluidization velocity, were investigated in this work. In all gas velocities, at least 1700 images were captured and analyzed, and the data of bubble and emulsion phases were extracted from these images. In Fig. 5 the standard deviation of the bed height fluctuations is plotted versus the number of images captured. Fig. 5 shows that the standard deviation of the bed height increases with the number of images and then gradually tends to a constant value that represents a reasonable number of images selected for statistical work.

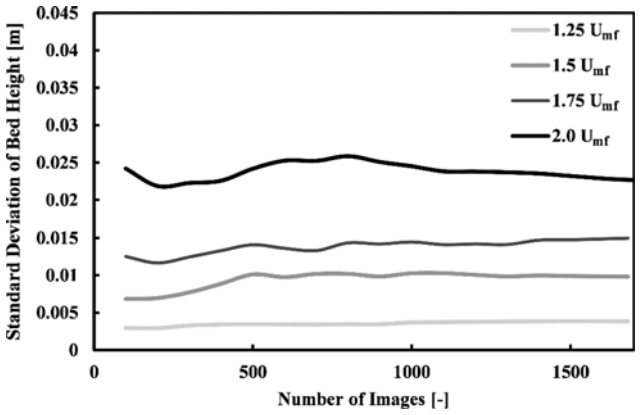

Fig. 5. Standard deviation of bed height versus number of images.

1. Bed Height

Figs. 6(a) and 6(b) show the variations of the dimensionless bed height and the bubble phase area in the bed versus time, respectively. The periodic and oscillatory behavior of dimensionless bed height and area of the bubbles are clearly visible in Figs. 6(a) and 6(b). The bubbles are the main reason for fluctuations of bed height. Some of the bed height fluctuations are due to bubble creation and their exit. Figs. 6(c) and 6(d) show a bubble exactly before and after leaving the bed, respectively. As shown in Figs. 6(a) and 6(b), when a bubble exits the bed, significant reduction is obtained in the values of dimensionless bed height and total area of the bubble phase. Naturally, small bubbles cause small fluctuations and big bubbles cause larger fluctuations. The most similarity between bed height fluctuations and total area of the bubbles in the bed is proof for this claim.

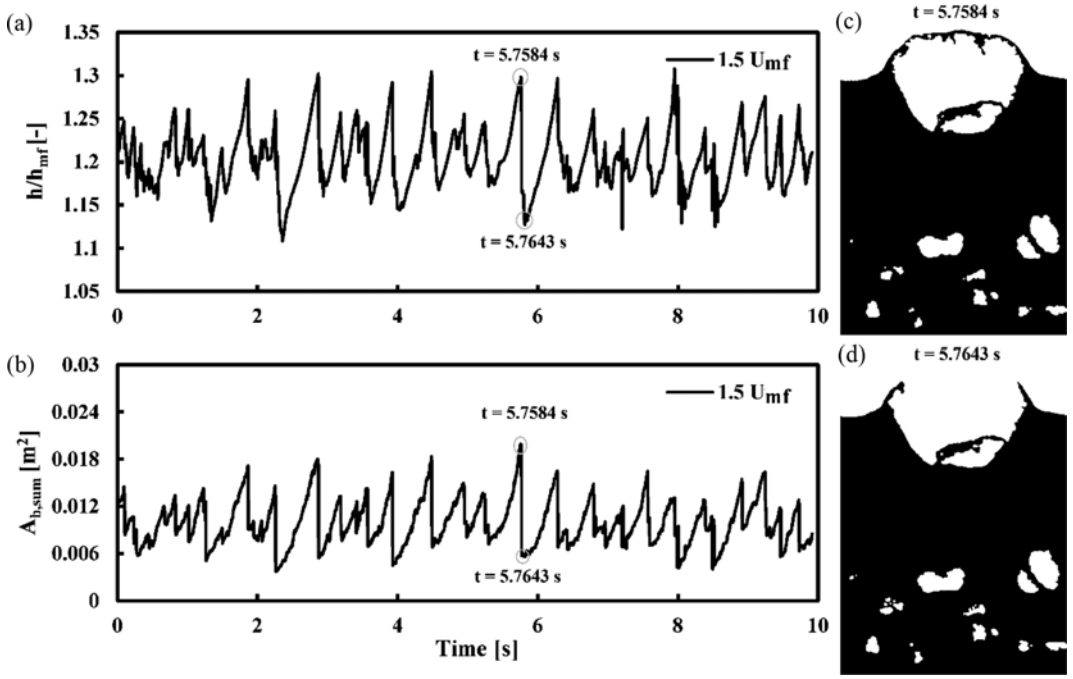

Fig. 6. (a) Fluctuations of bed height with time (b) fluctuations of summation of bubbles area in bed versus time (c), (d) corresponding images.

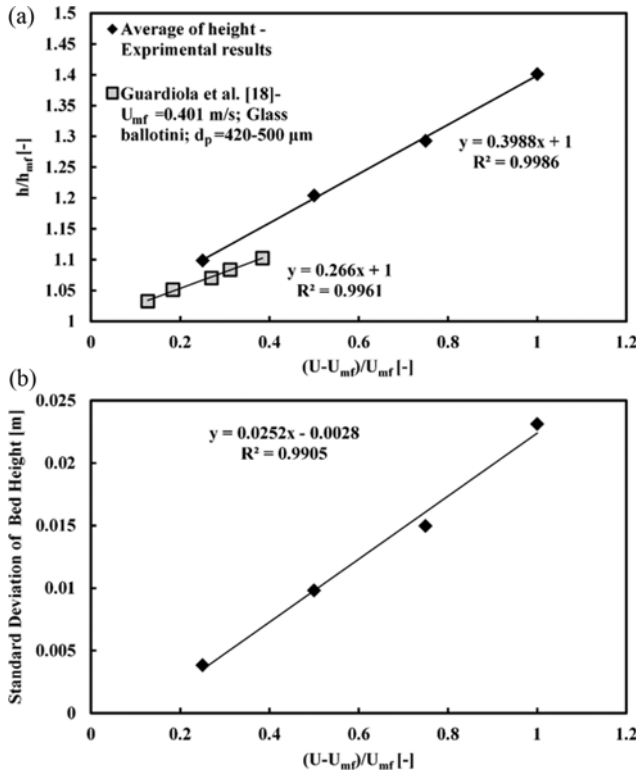

Fig. 7. (a) Averaged bed height and (b) standard deviation of the bed height versus dimensionless excess gas velocity.

Fig. 7(a) shows the variation of dimensionless bed height to dimensionless excess gas velocity (U_0–U_{mf}/U_{mf}), so that when excess gas velocity increases, the dimensionless bed height increases linearly. In addition, Fig. 7(a) shows that the slope of dimensionless bed height increment is about 0.4 for this type of particles. Fig. 7(a) presents a comparison between our results and the results presented by Guardiola et al. [18]. It can be understood that in their work the variation of bed height as a function of excess gas velocity is linear with the slope of 0.266. Busciglio et al. [14] reported that in higher gas velocities, the trend of bed height variations as a function of velocity is not linear anymore. Fig. 7(b) shows that the standard deviation of the bed height increases with gas velocity. Standard deviation of the fluidized bed height shows the fluctuation of the particles height around an average value. Standard deviation of the bed height may give us some information about the maximum height of the particles during the operation and could be used for fluidized bed design purposes.

2. Equivalent Bubble Diameter

Fig. 8 shows a comparison of the average bubble diameter and the bubble diameter obtained from a correlation presented by Shen et al. [12]. Their correlation is as follows:

$$d_b^{\frac{2}{3}} = \frac{8\left(2^{\frac{3}{4}}-1\right)(U_0-U_{mf})}{\lambda\sqrt{g}}\left(h+\frac{\lambda}{\pi\left(2^{\frac{3}{4}}-1\right)}\frac{A_0}{D}\right) \quad (4)$$

In the present work, the average bubble diameter obtained from DIA is defined on the basis of the following equation:

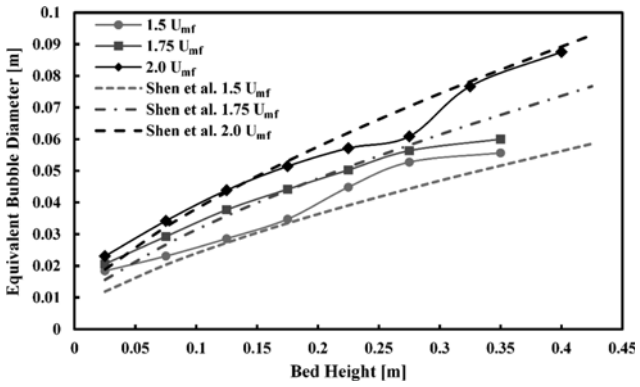

Fig. 8. Equivalent bubble diameter variations through the emulsion phase.

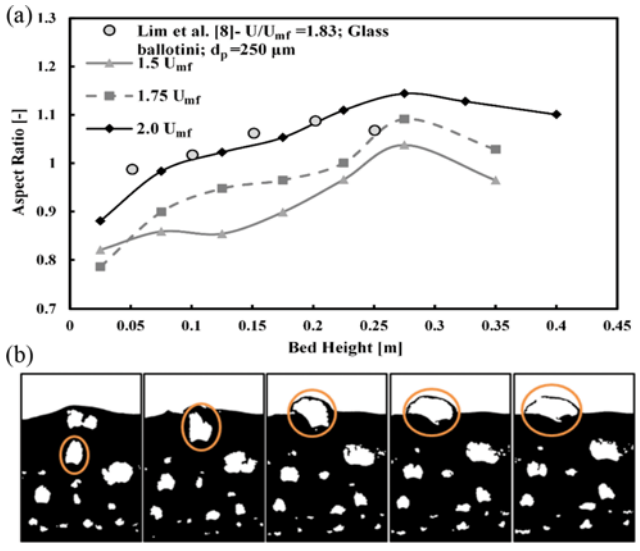

Fig. 9. (a) Aspect ratio of bubbles at different bed heights for different gas velocities (b) evolution of a tracked bubble at different bed heights.

$$d_b = \frac{\Sigma_{i=1}^{N_b} d_{b,i}}{N_b} \quad (5)$$

where N_b is the total number of bubbles in a rectangular control volume with the length of bed width and height of 2Δy (see Fig. 4). Here, the values of 0.025 and 0.05 m were taken for Δy and for last interval in each velocity, respectively. Fig. 8 shows good agreement between DIA results and predicted results using Eq. (4).

Fig. 8 shows how bubbles grow through the bed: bubble diameter increases with increasing fluidization gas velocity.

3. Bubble Aspect Ratio

Fig. 9(a) shows the averaged aspect ratio of the bubbles versus vertical position from gas distributor, along with the results reported by Lim et al. [8]. As a general result, it is obvious that in most of heights, by increasing the gas velocity, aspect ratio of bubbles increases. In each case, the aspect ratio value starts from values less than one, then rises and reaches a maximum value. The value of aspect ratio, then, passes the maximum value and decreases. The same trend was observed in other works such as

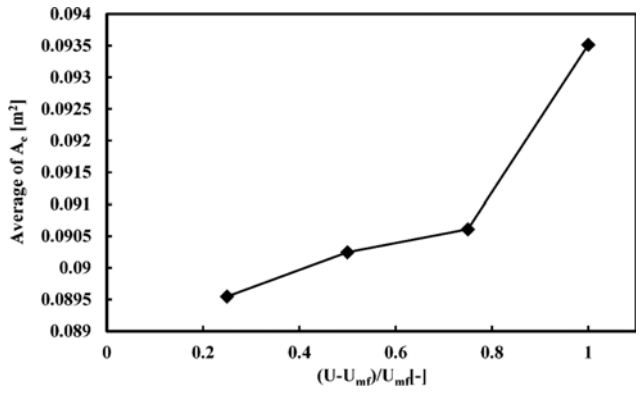

Fig. 10. Average of A_e variations with gas velocity.

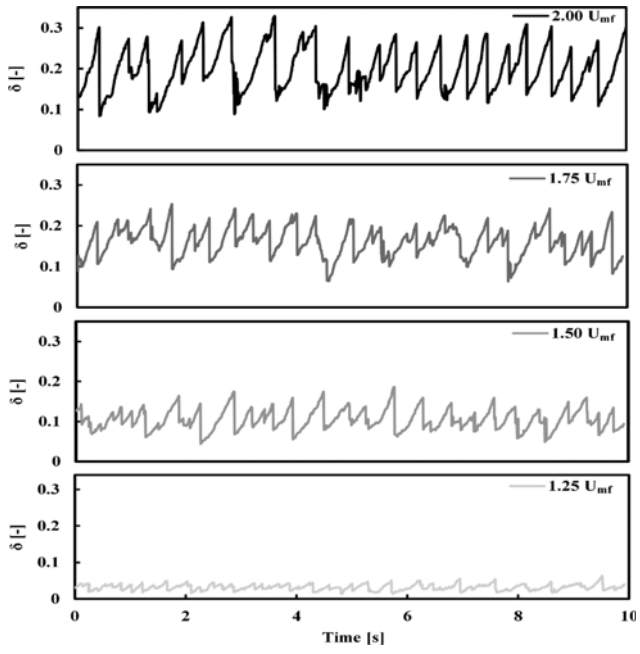

Fig. 11. δ Parameter variation in four velocity during time.

reported by Lim et al. [8], which can be seen in Fig. 9(a) and Asegehegn et al. [15]. In some cases, the aspect ratio decreases to values less than one. The main reason for decreasing the bubble aspect ratio near the bed freeboard is that in spite of typical bubbles inside the bed, the bubbles in this region are not influenced by the leading bubbles. As stated earlier, the bubbles inside the fluidized bed are elongated because of the bubble-bubble interactions effects induced mainly by the leading bubbles [23,24]. Moreover, as can be seen from Fig. 9(b), in spite of the bubbles inside the interior domain of the fluidized bed, the exiting bubbles are not in the squeezing effect of lateral emulsion phase, which permits these bubbles to be relaxed in lateral direction.

4. Area of the Emulsion Phase

Area of the emulsion phase is related to the gas velocity. In this section, a variation of A_e with gas velocity is presented. In Fig. 10, average values of A_e are plotted versus dimensionless excess gas velocity. The emulsion phase becomes more expanded at higher excess gas velocities. To describe this phenomenon, the variation

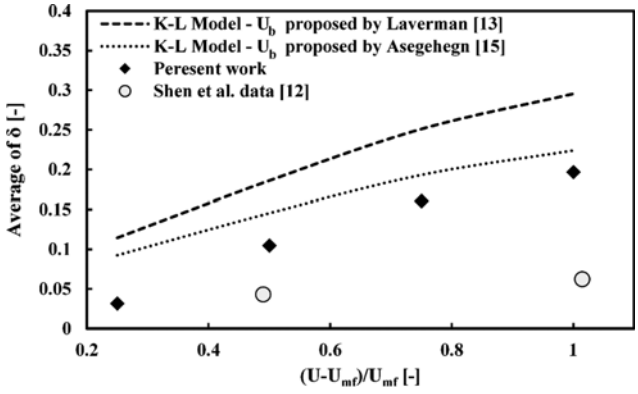

Fig. 12. Variations of average δ function with gas velocity.

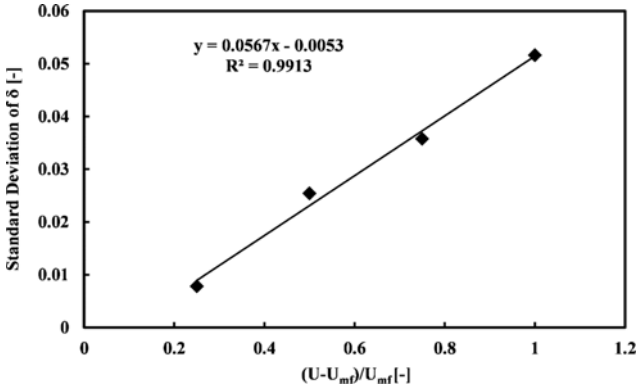

Fig. 13. Variations of standard deviation for δ parameter.

of the bubble fraction in the bed should be presented and discussed (see section 4.5).

5. Bubble Fraction in the Bed (δ)

The bubble fraction (δ) in the fluidized bed can be calculated using Eq. (3). Fig. 11 presents δ parameter fluctuations for different gas velocities: by increasing the gas velocity, fluctuations of δ parameter also increase. Figs. 12 and 13 show the average bubble fraction (δ), and its standard deviation versus excess gas velocity, respectively. In Fig. 13 the standard deviation of δ parameter increases when the gas velocity rises. It is also remarkable that the variation of the standard deviation of δ increases linearly with the excess gas velocity. The results of the averaged values for δ are compared with the data presented by Shen et al. [12].

Fig. 12 shows the prediction of K-L [1] model for δ parameter versus excess gas velocity using two different correlations for bubble rising velocities. The trend of the results is the same, but as can be observed from this figure, the results of the present work are more similar to the K-L model with the bubble rise velocity correlation of Asegehegn [15]. The K-L model with the bubble rise velocity of Laverman [13] predicts the results with a considerable over-estimation. On the other hand, our results are greater than the values reported by Shen et al. [12]. The data points presented by Shen et al. [12] are for particles with an average diameter of 0.46 mm, which is considerably smaller than the LLDPE particles used in this work. As Shen et al. [12] stated, the bubble density increases with the particle size; thus, it can be concluded that the bub-

ble density and consequently the δ parameter becomes greater for our particles.

As can be observed from Fig. 12, the rate of growth for δ parameter is decreasing with increasing the excess gas velocity. By considering Eq. (3), because the term (A_e) has an ascending trend (Fig. 10) with excess gas velocity, it can be concluded that at higher excess gas velocities more excess gas is presented in the dense phase.

By comparison of Figs. 8 and 12, while bubble diameter is in quite good agreement (Fig. 8) with the data reported by Shen et al. [12], δ seems quite different (Fig. 12). The average bubble diameter reported in the present work is the arithmetic average of bubble diameter ($d_{b,10}$). In this averaging method the weight of each bubble in the averaging procedure is the same. The δ parameter relates to the bubble area, which in turn is proportional to d_b^2. Fig. 14 shows both the arithmetic averaged bubble diameter ($d_{b,10}$) and area weighted bubble diameter ($d_{b,21}=\frac{\Sigma_{i=1}^{N_b} d_{b,i}^2}{\Sigma_{i=1}^{N_b} d_{b,i}}$) versus bed height. In the second averaging method the weight of larger bubbles is greater than the weight of small ones. As can be observed from this figure, the deviation of the $d_{b,21}$, from Shen et al. [12] averaging procedure is more noticeable at higher elevations due to the presence of larger bubbles.

Fig. 15 shows the variation of the δ parameter versus vertical position: by increasing the bed height the δ parameter is decreased.

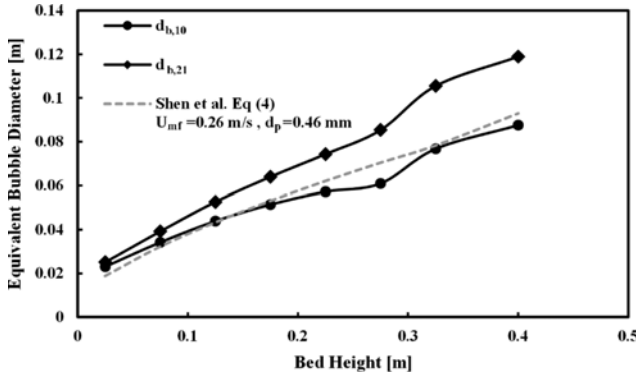

Fig. 14. Comparison between averaging methods for equivalent bubble diameter.

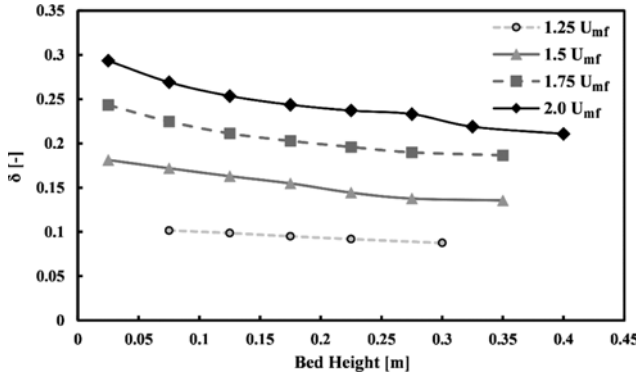

Fig. 15. Variations of δ parameter in bed height.

It may be attributed to more leakage of the gas from the large bubbles at higher elevations to the dense phase.

CONCLUSIONS

An experimental study was done in a pseudo-2D gas solid fluidized bed with Geldart B type of particles using DIA technique and the following results were obtained:

- The bed surface fluctuation analysis shows that the bed average height increases linearly with the gas velocity. Moreover, the bed surface fluctuations have a linear trend with the excess gas velocity.
- There is a maximum value for aspect ratio near the freeboard. Actually, bubbles get wider near exit points. The main reason for decreasing the bubbles aspect ratio in this region is that in spite of typical bubbles inside the bed, the bubbles in this region are not influenced by the leading bubbles. Thus, the bubbles inside the bed are elongated because of the bubble-bubble interaction effects induced mainly by the leading bubbles. Moreover, in spite of the bubbles inside the interior domain of the fluidized bed, the exiting bubbles are not in the squeezing effect of lateral emulsion phase, which permits these bubbles to be relaxed in lateral direction.
- The dense phase became less dense at higher excess gas velocities. The trend is in correspondence with the data obtained for bubble fraction in the bed (δ). δ parameter getting increased by gas velocity rising in the fluidized bed.
- At higher bed elevations, the volume of gas presented in the dense phase was increased. This is related to the presence of larger gas bubbles and the increased gas leakage from bubble to the emulsion phase at higher bed elevations.

NOMENCLATURE

A : area [m^2]
D : depth of bed [m]
H : height of bed [m]
N : number of bubbles [-]
U : velocity [m/s]
W : width of bed [m]
a : maximum width of bubbles [m]
b : maximum height of bubble [m]
d : diameter [m]
g : gravitational acceleration [m/s^2]
h : height of emulsion phase in bed [m]
r : direction [m]
t : time [s]
u : velocity [m/s]
y : position in the bed in y direction [m]

Greek Symbols

δ : bubble fraction in bed [-]
λ : constant in shen et al. equation
ρ : density [kg/m^3]

Subscripts

o : orifice position

b : bubble
bed : bed
e : emulsion
f : freeboard
i : index
mf : minimum fluidization condition
pix : pixel
p : particle
sum : summation
t : total

SUPPORTING INFORMATION

Additional information as noted in the text. This information is available via the Internet at http://www.springer.com/chemistry/journal/11814.

REFERENCES

1. D. Kunii and O. Levenspiel, *Fluidization Engineering*, Elsevier (2013).
2. J. Nieuwland, M. Veenendaal, J. Kuipers and W. Van Swaaij, *ChEnS*, **51**, 4087 (1996).
3. O. Olaofe, K. Buist, N. Deen, M. van der Hoef and J. Kuipers, *Powder Technol.*, **244**, 61 (2013).
4. A. Busciglio, G. Vella, G. Micale and L. Rizzuti, *Chem. Eng. J.*, **140**, 398 (2008).
5. S. Mori and C. Wen, *AIChE J.*, **21**, 109 (1975).
6. P. Rowe and B. Partridge, *Chem. Eng. Res. Des.*, **75**, S116 (1997).
7. J. Kuipers, W. Prins and W. Van Swaaij, *ChEnS*, **46**, 2881 (1991).
8. K. Lim, P. Agarwal and B. O'neill, *Powder Technol.*, **60**, 159 (1990).
9. A. S. Hull, Z. Chen, J. W. Fritz and P. K. Agarwal, *Powder Technol.*, **103**, 230 (1999).
10. G. R. Caicedo, J. J. P. Marqués, M. G. Ruız and J. G. Soler, *Chem. Eng. Process.*, **42**, 9 (2003).
11. M. Goldschmidt, J. Link, S. Mellema and J. Kuipers, *Powder Technol.*, **138**, 135 (2003).
12. L. Shen, F. Johnsson and B. Leckner, *ChEnS*, **59**, 2607 (2004).
13. J. A. Laverman, I. Roghair, M. v. S. Annaland and H. Kuipers, *CJChE*, **86**, 523 (2008).
14. A. Busciglio, G. Vella, G. Micale and L. Rizzuti, *Chem. Eng. J.*, **148**, 145 (2009).
15. T. W. Asegehegn, M. Schreiber and H. J. Krautz, *Powder Technol.*, **210**, 248 (2011).
16. S. Movahedirad, A. Molaei Dehkordi, M. Banaei, N. Deen, M. van Sint Annaland and J. Kuipers, *Ind. Eng. Chem. Res.*, **51**, 6571 (2012).
17. S. Movahedirad, M. Ghafari and A. Molaei Dehkordi, *Chem. Eng. Technol.*, **37**, 103 (2014).
18. J. Guardiola, G. Ramos and R. Elvira, *ChEnS*, **95**, 33 (2013).
19. D. Geldart, *Powder Technol.*, **7**, 285 (1973).
20. J. Link, L. Cuypers, N. Deen and J. Kuipers, *ChEnS*, **60**, 3425 (2005).
21. C. A. Schneider, W. S. Rasband and K. W. Eliceiri, *Nat. Methods*, **9**, 671 (2012).
22. T. Ridler and S. Calvard, *ITSMC*, **8**, 630 (1978).
23. S. Movahedirad, M. Ghafari and A. M. Dehkordi, *Chem. Eng. Technol.*, **35**, 929 (2012).
24. S. Movahedirad, A. Molaei Dehkordi, N. G. Deen, M. van Sint Annaland and J. Kuipers, *AIChE J.*, **58**, 3306 (2012).

Supporting Information

Some general aspects of a gas-solid fluidized bed using digital image analysis

Mahdi Salehi-Asl, Saeed Azhgan, and Salman Movahedirad†

School of Chemical Engineering, Iran University of Science and Technology, P. O. Box 16765-163, Tehran, Iran
(*Received 8 April 2017 • accepted 15 October 2017*)